2025 IEEE International Conference on Robotics and Automation (ICRA)
May 19-23, 2025. Atlanta, USA

Analysis of kinematics and propulsion of a self-sensing multi-DoF undulating soft robotic fish

Myungsun Park[1], Jacobo Cervera-Torralba[1], Iman Adibnazari[1], Geno Pawlak[1,2] and Michael T. Tolley[1,3]

***Abstract*— In this paper we explore kinematics ranging from anguilliform to thunniform achieved in a self-sensing multi-degree-of-freedom soft robotic fish and analyze the effect of them on the swimming. First, we examine the characteristics of the bending actuators of the robotic fish. Then, we express the kinematics of the fish as a propagating wave parameterized by three bending amplitudes and a wavelength, which are determined by the flow rates and phase shift of the pumps. We capture various motion patterns generated by different actuator inputs and directly measure the thrust generated by each pattern. We observe that the robotic swimmer can reproduce two different modes of propulsion, that are embodied by two distinct morphological patterns in nature: anguilliform and thunniform. When neither of modes are activated, propulsion is zero or even negative. Finally, we estimate the stationary swimming speed by towing the undulating fish, which satisfies the slip condition (with the speed of the body wave matching the swimming velocity). The analysis of a wide range of kinematic patterns in this study, including two extreme cases of anguilliform and thunniform modes, will provide insights for comprehensive understanding the mechanics of efficient swimming.**

I. Introduction

Biological fish propel themselves by undulating (i.e., bending parts of their body at specific timing to generate thrust) to push against the water. This fluid-body interaction is affected by a variety of factors, including the hydrodynamic condition of the surrounding flow [1], the anatomy of the skeletal system, the kinematics determined by distributed muscle activation [2], and the mechanical properties of the skin [3]. For decades, robotics has played an important role in understanding these complex interactions. A conceptual or functional analogue of the fish (i.e., a robotic fish) allows us to observe and control a wide range of the variables of interest [4]. For example, we can directly measure variables that are otherwise difficult to observe with animals, such as the thrust they generate or the drag they experience while moving through water. Conversely, the knowledge acquired with these "biorobotic" studies [4] promotes the development of underwater robotic systems with improved performance [5], [6], [7], [8]. One important space of research into biological swimming relates to how fish control their kinematics to generate thrust. Research has revealed much about the relationships between morphology of their bodies or fins, kinematics, and generated thrust [9]. Based on these findings, various robotic fishes have been developed [10], [11], [12], [13].

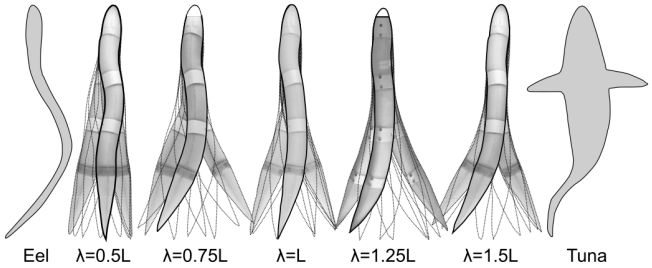

Fig. 1. Superimposed images and silhouettes of the robotic fish with various wavelengths (λ=0.5L, 0.75L, L, 1.25L, 1.5L) in one tail-beat cycle (L: Length of the body).

Despite these advances, there is still a critical gap between the performance of biological swimming and its robotic replications. Biological fish use the muscles distributed along their bodies to orchestrate bending that results in traveling waves that propagate from their heads to their tails [14], [10], [15]. The shape and speed of the traveling waves are determined by when (muscle activation time) and how much (bending angle) fish bend parts of the body. Researchers have observed wide variation in these kinematics between species [16] and have studied their effects on swimming performance. One study proved that nearly every muscle contributes to propulsion for all species [14], while another observed that fishes rarely activate the anterior muscles when they are swimming slowly [17] and only the posterior part of the body contributes in producing vorticity [9].

These comparative approaches to investigate the complex kinematics in biological fishes, however, have limitations. Most significantly, it is hard to compare kinematics between species that have different anatomies [14]. The field of biorobotics proposes a resolution to this problem by developing a platform that can independently control multiple segments of the body [18]. A study with an array of fluidic actuators that mimicked an eel related the overall undulatory amplitude of the swimmer to the thrust, while keeping the wavelength constant [19]. The effect of the wavelength on swimming was reported by two individual works on a pneumatically driven soft robot [13] and a rigid robot with multiple servomotors [20]. The former work also found that the anterior motion affected the swimming velocity and

This work was supported by the Office of Naval Research, grants number N00014-22-1-2595 and N00014-23-1-2169.

[1]These authors are with the Department of Mechanical and Aerospace Engineering, University of California San Diego, 9500 Gilman Dr, La Jolla, CA 92093 USA. mypark,jcerveratorralba,iadibnaz,epawlak,tolley@ucsd.edu

[2]Geno Pawlak is also affiliated with Scripps Institution of Oceanography, UC San Diego.

[3]Michael T. Tolley is also affiliated with the Materials Science and Engineering Program, UC San Diego.

2025 IEEE International Conference on Robotics and Automation (ICRA) | 979-8-3315-4139-2/25/$31.00 ©2025 IEEE | DOI: 10.1109/ICRA55743.2025.11127497

efficiency [13]. However, none of the these examined the performance while all the segments along the body were independently controlled. Also, all these works evaluated performance based on the swimming velocity but did not directly measure the thrust generated.

In this study, we leverage a custom soft robotic fish with three independently controllable segments to explore the multi-DoF swimming kinematics and their effect on underwater propulsion. We approximate the complex kinematics observed in biology as a combination of nonuniform bending angles of the segments and overall wavelength. The robotic fish presents various wave propagation patterns (Fig. 1) depending on these kinematic parameters. To evaluate how these parameters affect the performance, we directly measure the thrust and discuss the relation of the shape of the undulation to the propulsion. We also estimate its swimming speed by measuring the forces while towing the undulating robotic fish through water.

II. Self-Sensing Hydraulic Bending Actuator

In this section, we describe the design of the actuator modules with embedded sensors that make up the robotic fish and enable multi-DoF bending with real-time observation. The design and fabrication of the actuators builds on our previous work [21], in which we proposed a method to ensure consistent fabrication of the actuator modules and demonstrated a preliminary version of the assembled robot. In the current work, we modified this module design to add a bending sensor for closed-loop control and fault detection and integrated a hydraulic subsystem and controllers into the system. In the later sections, we test the assembled robotic fish generating a variety of swimming motions (see Fig. 1). In this section, we first examine the bending motions of the actuator module and the response of the sensor to different oscillation frequencies.

A. Design and bending motion

Fig. 2(a) shows the design of the actuator with the embedded bending sensor. The details of the design and fabrication, especially of the internal chambers that are filled with water that drive the bending motion, are similar to those that we have reported previously [21]. The two internal chambers were connected through a hydraulic pump (MGD1000 Series F, TCS Micropumps) that sends water from one side to the other to create a bending motion by expanding or contracting the volume of each chamber. A commercially available bending sensor (Bi-directional Flex Sensor, Flexpoint Sensor Systems) was attached to the flexible constraint layer at the center of the actuator with flexible adhesive (Loctite Vinyl, Fabric & Plastic Repair, Loctite). We assumed that the central axis of the actuator bent with a constant curvature [2], [21]. We defined the bending angle of an actuator as the central angle of the arc formed by the central axis (see Fig. 2(b)). In the neutral position (straight), the bending angle was defined to be zero.

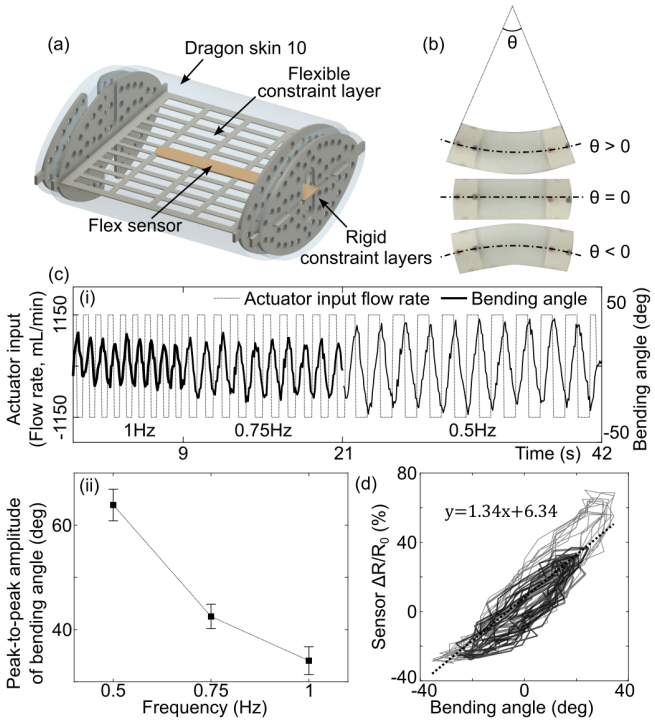

Fig. 2. Characterization of the self-sensing bending actuator. (a) Design of the actuator. (b) Bending angle defined as the central angle of the arc created by the actuator. (c) Time series (i) and peak-to-peak amplitudes (ii) of the bending angles of the actuator oscillating in three different frequencies (0.50, 0.75, 1.00 Hz). The error bars represent the standard deviations. (d) Corresponding sensor signals (change of the resistance divided by the initial resistance, $\Delta R/R_0$) during the oscillations with the best fit line by least-squares method.

B. Frequency response

Fig. 2(c) shows the time series (i) with peak-to-peak amplitudes (ii) of the bending angle of the actuator under a constant water flow input (1150 mL/min) that was switching direction at three different frequencies (1.00 Hz, then 0.75 Hz, then 0.50 Hz). From the time series, we confirmed that the bending angle was continuously increasing or decreasing with time before flow switched direction for each frequency. Therefore, the peak-to-peak bending angle became smaller as the frequency increased. Based on this observation and considering the limited maximum flow rate (1150 mL/min) of the pump, we decided to operate the actuators at the lowest frequency (0.5 Hz) for the rest of this study to allow them to achieve sufficiently large bending angles for swimming.

The resistance of the sensor increased or decreased depending on the change of the bending angle in two ways (see Fig. 2(d)). First, the sensitivity was different for each direction, which is due to the mechanism of the sensor that measures the change of the resistance caused by the microcracks in the conductive ink coated on the thin film [22]. Second, we observed hysteresis dependent on the rate of actuation, which must be considered for accurate estimation of the bending angles.

III. Multi-DoF Kinematics

In this section, we discuss the multi-DoF kinematics of the undulating robotic fish. We generated various waveforms along the body by varying the inputs to the three actuators (see Fig. 1). We first model these multi-DoF kinematics, and then through experiments, we investigate the wide range of kinematic modes of swimming that our robotic fish can generate.

A. Kinematic parameters

In the literature, time-varying undulation of a swimming fish has often been approximated as a sinusoidal wave [23]

$$y(x,t) = a_1(x) sin 2\pi(ft - \frac{x}{\lambda}), \quad (1)$$

where y is the displacement of the midline, x is the position along the body length, $a_1(x)$ is the amplitude of the undulation, f is the frequency of oscillation, and λ is the wavelength. Throughout this work, as mentioned in Section II, we fixed the frequency of oscillation to be 0.5 Hz. The amplitude and the wavelength of the undulation in our robotic fish depend on the bending angles and the phases of the three actuators, respectively. Then, the kinematics of the robotic fish can be described as follows:

$$y(x,t) = a_2(x|\theta_1, \theta_2, \theta_3) sin(\pi t - \phi(x)), \quad (2)$$

where θ_1, θ_2, θ_3, and $\phi(x)$ represent the maximum bending angles and the phases of the actuators. We can manipulate these kinematics by changing the rates of flow of water into the actuators (A_i) and the phase differences (ϕ) between them, i.e.,

$$\theta_i = \theta_i(A_i); \lambda = (2\pi/\phi)L_a, \quad (3)$$

where L_a is the length of the actuator. In other words, we input the flow rates (A_i) and the phase differences (ϕ) to control the bending angles (θ_1, θ_2, θ_3; and thus the amplitudes of the lateral motion) and the wavelength (λ) of the undulating fish.

B. Experimental setup and assembled robotic fish

To measure the correlation between kinematics of the robotic fish, and the corresponding thrust force, we developed a custom robotic testbed (see Fig. 3). We fixed the head of the robotic fish in a water tank to a robotic arm (UR16e, Universal Robots). Between the arm and the fish, we placed a load cell (F/T Sensor Delta, ATI Industrial Automation) to measure the forces acting on the fish (see Section IV). To capture the bending angles of each segment, we used a tilted mirror below the water tank to reflect the bottom of the fish and recorded videos of it using a camera. The robotic fish was structured with a rigid head, three actuators, and a passive tail, that were connected in series by rigid couples. Each actuator was in the form of an elliptic cylinder with a major axis of 66 mm, a minor axis of 40 mm, and a length of 80 mm. The couples were 12 mm long. The total length of the fish was 428 mm from the head to the tail. At each couple, we attached two tracking markers to calculate the bending angles of the actuators from the captured video.

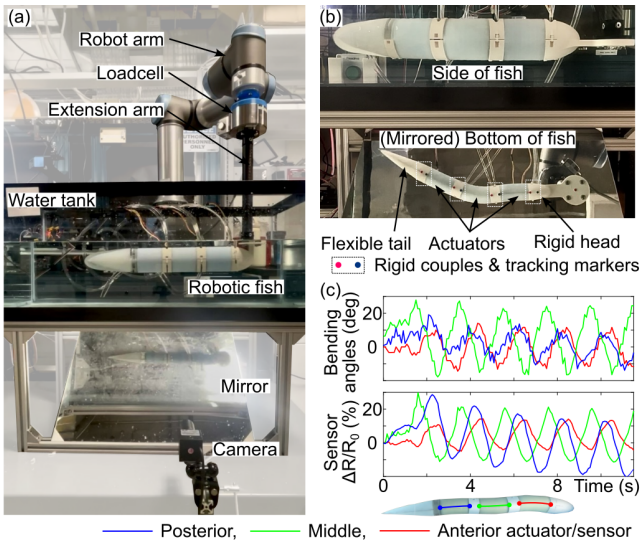

Fig. 3. Experiment for characterization and evaluation of the swimming performance of the robotic fish. (a) Setup for measuring the kinematics and the forces while the fish was undulating and/or towed by a robot arm. (b) Side and bottom view of the assembled robotic fish. (c) Representative time series of the bending angles and corresponding sensor signals measured from the three actuators of the robot during the experiment.

Fig. 3(c) shows an example of the calculated bending angles and the corresponding sensor signals collected while the fish was swimming.

C. Results

As previously mentioned, the kinematics of the robotic fish were determined by the rates of flow of water into the actuators and the phase differences between each, resulting in varied bending angles and wavelengths. To explore the effect of these actuator inputs on the kinematics, we graphically compared the trajectories of the mid-line of the fish generated by a wide range of inputs (Fig. 4).

We first selected five phase differences (π, $2\pi/3$, $\pi/2$, $2\pi/5$, $\pi/3$) that resulted in five wavelengths ($0.5L$, $0.75L$, L, $1.5L$, $2L$, where L is the length of the body). We then defined four combinations of the flow rates that resulted in four representative distributions of amplitudes of the lateral motion of the three actuators: balanced; anterior-focused; middle-focused; and posterior-focused flow rate distributions (see Table I). We set the sum of the flow rates of the actuators to be constant, so that we could compare the kinematics independent from the total power input.

We examined the kinematics according to these actuator inputs in simulation and experiment. Fig. 4(a) shows the

Flow rate (mL/min)	Posterior actuator	Middle actuator	Anterior actuator	Sum
Balanced	383	383	383	1150
Anterior-focused	128	383	639	1150
Middle-focused	256	639	256	1150
Posterior-focused	639	383	128	1150

TABLE I

Combinations of the water flow rates for three actuators.

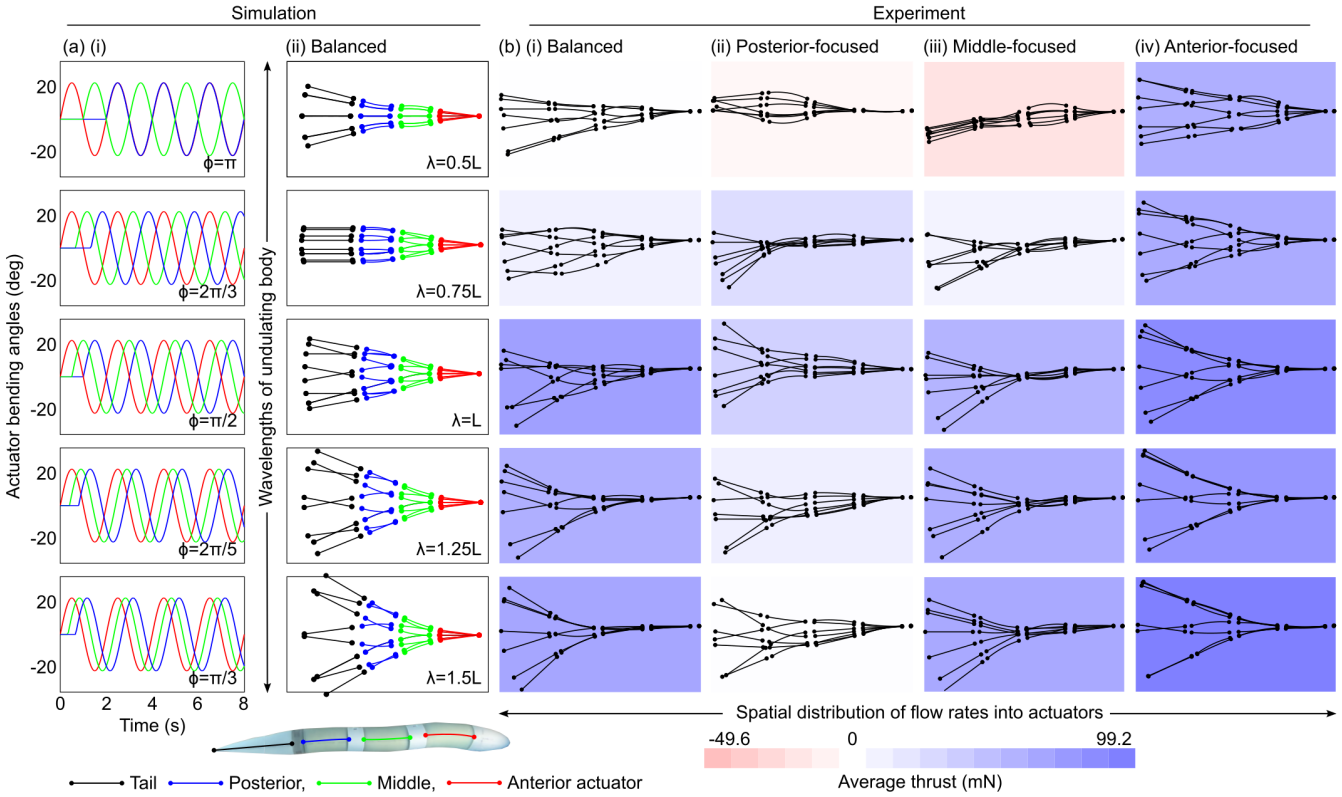

Fig. 4. Mid-line kinematics of the robotic fish and generated thrusts. (a) Simulated mid-line kinematics of the robotic fish. Time series of the input bending angles of the three actuators with balanced flow rate (see Table I) and five phase shifts (i), resulting in distinct mid-line kinematics with five different wavelengths (λ=0.5L, 0.75L, L, 1.25L, 1.5L) (ii). (b) Experimentally measured mid-line kinematics of the robotic fish for various inputs to the actuators. Each row represents the different wavelength of the undulating body, while each column represents a different distribution of flow rates to the modules: balanced (i), posterior-focused (ii), middle-focused (iii), and anterior-focused (iv). The background color of each subfigure represents the average thrust generated in one tail beat cycle, as is discussed in Section IV.

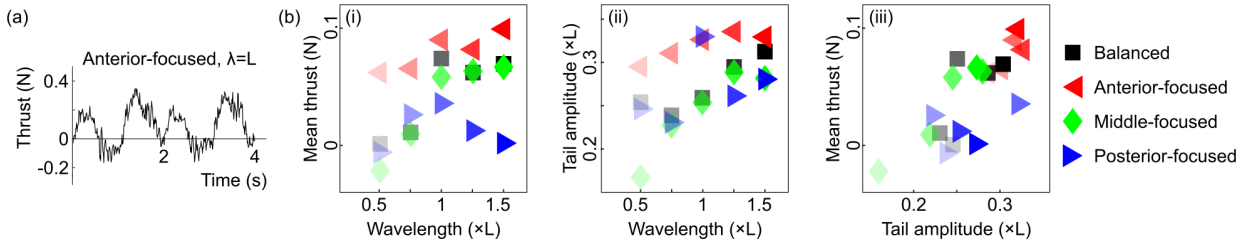

Fig. 5. Thrust generated by the undulating robotic fish with a fixed head. (a) Representative time series of the thrust ($\lambda = L$, anterior-focused actuation). (b) Average thrust generated in two tail beat cycles with five wavelengths and four combinations of flow rates.

time series of bending angles and resulting trajectories of the mid-line of the fish in one tail beat cycle, given the five wavelengths and balanced flow rates. Even though the total flow rate into the actuators was the same in each case, they displayed completely different kinematics. In particular, the amplitude of the tail fluctuation—which plays an important role in pushing water backward and propelling the body forward—varied widely. This variation suggests we should expect a similarly large variation in propulsion, which we discuss in the next section.

Fig. 4(b) depicts the the experimental mid-line kinematics exhibited by our robotic fish. First of all, the results for balanced flow rates (i) were similar to the results from the simulation, which implies that the robotic fish could reproduce the desired motion well. A dominant cause of the simulation-to-reality gap that still existed would be the resistance and damping from the water and the inherent asymmetry of the robot.

As with the simulation, the experiments revealed a variety of kinematics, including in the amplitude of the tail motion. Especially in the case of λ=0.5L, there were two characteristics that distinguished it from the other cases. First, the undulation of the fish was almost stationary and did not propagate along the body (see the supplementary video). This observation allowed us to infer the boundary conditions of the undulation, which were obviously closed at the fixed head as well as at the interface between the posterior actuator and the tail. Second, in the case of the posterior-focused or

middle-focused flow rates, the lateral amplitude of the tail was smaller than that of the anterior bodies, which does not appear in biological fishes. Each of these two distinct characteristics had a negative effect on propulsion, which will be discussed more in detail in the next section.

IV. Thrust, Drag, and Free-Swimming Velocity

A. Experiments overview

Swimmers that undulate their bodies, including our robotic fish, generate thrust by propagating waves along their body in the direction opposite to the direction of motion. These waves generate vortical structures along the body that form a jet comprised of vortex pairs that propagate downstream. Depending on the ratio of the swimming velocity (U) to the speed of the wave (V), which is referred to as the slip (U/V), they enable both acceleration and deceleration [24]. Biological fish control their locomotion by adjusting the slip; for example, they increase the speed of the traveling wave to be larger than their swimming velocity to accelerate. On the other hand, when the slip is larger than or equal to one, they decelerate or swim at a constant velocity.

In this section, we evaluate the propulsion of the robotic fish in two ways using the load cell and the robot arm in Fig. 3. First, without relative movement between the fish and the flow (U=0), we measure the thrust generated by the fish according to the kinematics presented in Section III. This allows us to focus on the effect of the kinematics on thrust by minimizing other hydrodynamic effects induced by the undulation. Second, we tow the undulating fish at different speeds and find the speed when the net force is zero. This speed is assumed as an estimated free swimming speed, and then we compare this to the speed where slip becomes one (U=V).

B. Fixed propulsion

We measured thrust while the fish was undulating its body with the range of inputs (combination of flow rates and wavelengths of undulation) described in Section III and Fig. 4, with its head being fixed. Fig. 5(a) is an example of the time series of the thrust for anterior-focused flow rates with wavelength of undulation λ=L. We observed two peaks in one tail beat cycle (2 seconds) corresponding to the left and right tail beats. Because of the asymmetry associated with starting flow, the first peak is weaker than the second and this pattern persists for later beats.

Fig. 5(b) shows the average thrust in two tail beat cycles, which was also represented as a background color in Fig. 4. The most notable result was that the anterior-focused actuation (represented as red markers) generated large thrust regardless of the wavelengths, even including λ=0.5L which, as we mentioned in Section III, generated a stationary wave. We attribute this result to the fact that the anterior actuator, which is farthest from the tail, can always generate a large fluctuation of the tail (see Fig. 5(b)(ii)). This lateral motion of the tail allows shedding of strong vortex pairs behind the body, which are typically observed in thunniform swimming mode for species like tuna [25]. This is distinct from the continuously propagating waves in motions of anguilliform swimmers such as eels. We found the lateral amplitude of the tail had a strong positive effect on the thrust generated (see Fig. 5(b)(iii)). We expect that the influence of the oscillating tail on the thrust (represented in red markers in the figure) was as important as that of the propagating wave (represented as black and green markers with relatively small tail amplitudes but comparable thrusts).

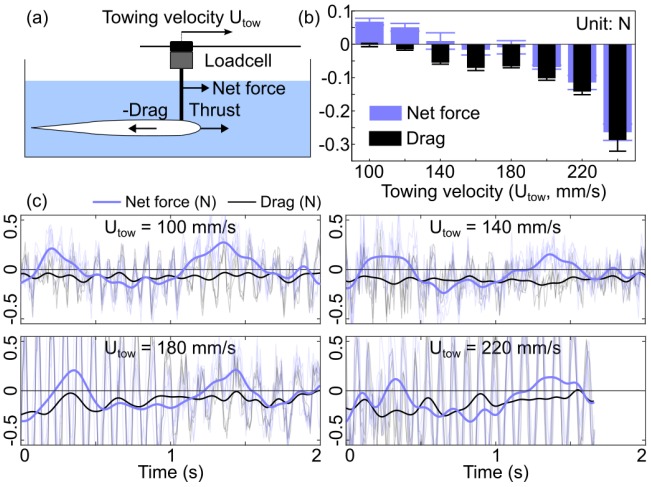

Fig. 6. Towed propulsion test for measuring net forces and drags on the robotic fish being towed underwater with (net force) and without (drag) anterior-focused flow rate and $\lambda = L$. (a) Schematic of the test. (b) Bar graphs on the time-averaged net force and the drag during two tail beat cycles. The error bars represent the standard deviations. (c) Time series of forces while towing the fish with four velocities. Thin curves represent five (net force) and three (drag) repeated measurements. Thick curves represent the averages of the repetitions, each of which were low-pass filtered with cut-off frequency of 2 Hz to remove vibration of the robot arm.

In the same context, for the case of the negative thrust for middle-focused and posterior-focused flow rates with λ=0.5L which we briefly discussed in Section III, there was little tail fluctuation and the wave was stationary, so little thrust would have been generated since neither the thunniform nor anguilliform propulsion were engaged. Moreover, the lateral motion of the central part of the body may result in a forward propagating vortex pair with an associated negative thrust.

C. Towed propulsion

We then evaluated the performance of swimming when there was a relative motion to the water. We towed the undulating fish with constant velocities while measuring the net force (Fig. 6(a)). We selected the anterior-focused flow rate and λ=L. The colored bars in Fig. 6(b) represent the time average of the net force during two tail beat cycles (the time series are in Fig. 6(c)). The positive sign indicates force in the forward direction. The net force became more negative as towing velocity increased, since the drag which increases in the negative direction as velocity becomes larger is added to the thrust determining the net force as:

$$F_{net} = F_{thrust} + F_{drag}. \quad (4)$$

To estimate the effect of drag, we conducted the same experiment on the robot with all the actuators turned off

(black bars and curves in Fig. 6(b) and (c)). However, the separation of thrust or drag is more complicated than this approach because of the passive flapping or vortex shedding; the fluctuation in flow would lead to a larger drag than the one in the static case.

Based on the measured net forces, we predict a free-swimming velocity of the robot to be 140–180 mm/s, around which speed the average net force vanishes. This is consistent with slip theory, which predicts that the free-swim velocity should be the same as the propagating speed of the undulation, $V = f\lambda$ =(0.5 Hz)(368 mm)=184 mm/s.

V. Discussion

A. Swimming kinematics and thrust generation

In this study, we developed a modular soft robotic fish that approximated the undulation of biological fishes, explored the range of kinematics it could generate, and observed the effect of the kinematics on propulsion by directly measuring the forces. We found two distinct kinematics that generated large thrust, which were analogous to the two swimming modes found in nature: anguilliform and thunniform. This observation is consistent with the conclusion of a study that separated the kinematics of fishes into two groups of anguilliform and the rest [26].

The relationship between the kinematics and thrust in a robotic fish, which is the main scientific finding of this study, has been examined by either experimental or simulation-based approaches. The experimental approaches were mostly aiming at the motion driven by the caudal fin or posterior part. Therefore, only the effects of the related parameters, such as tail beat frequency [27], morphology and compliance [28], [29], were of interest. The importance of the length and amplitude of the body wave, which also considers the bending of the anterior part, has only been investigated in terms of the swimming speed [30], [13]. The direct evaluation of the thrust depending on those parameters has only been investigated by numerical simulations [31], [32]. These works predicted that a longer wavelength produces a larger thrust; we observed that this was only true in balanced, anterior-focused, and middle-focused actuations (Fig. 5(b)) but not in the posterior-focused case. The discrepancy may come from the different lateral amplitudes ($a_1(x)$ in Equation 1) in the studies. It connotes the importance of the spatial distribution of the actuation to the thrust in a robotic swimmer and opens room for further investigations.

B. Segmented body

The robotic fish in this study used three bending segments to generate various patterns of undulation. Biological fish, on the other hand, control their continuously distributed muscles with complicated spatial and temporal patterns to generate versatile motions [14]. Researchers have suggested different methods to recreate this complex movement in various robotic systems [33], [34], [35], [36], [37], [30]. Some of them could mimic the midline kinematics of fishes using less than or equal to four rotation joints [26], [38], or with two bending segments [39], while the relation between the number of segments and achievable kinematic range has not yet been evaluated.

Regardless of the structural variations, all the discrete approximations require properly controlled actuation for better swimming. For example, for this work, the time trajectory of the three bending angles has to be thoroughly designed to achieve a target motion. Here, as shown in Fig. 2(c), we simply operated the pumps with a constant flow rate to make a triangular trajectory. For more sophisticated motions, the embedded bending sensors could enable the closed-loop control of actuators to follow different trajectories depending on engineering goals such as biological similarity, swimming efficiency, etc.

C. Opportunities for future work

1) Free swimming: In this study, we fixed the head of the fish to measure the forces while it was undulating. In fact, fishes engage their heads in motion to start, to swim, or to align the body to minimize energy expenditure [40], [41]. The constraint in the head motion might have simplified the overall motion and resulted in linear relation between the thrust and the tail amplitude regardless of the wavelength (Fig. 5(b)(iii)). Future work could fill this gap by letting the swimmer freely move. However, a direct measurement of the forces would not be possible in this case, and accurate hydrodynamic simulations would be required to predict them.

2) Hydrodynamic considerations: As noted previously, thrust generation in fish swimming is associated with coupling between undulating motions and vorticity generated along the body. The propagation of these vortices and the associated thrust is likely to be modified by a nonzero swimming velocity ($U \neq 0$). On top of the experimental results of the towed propulsion test in this study, analysis of the kinematics of the robotic fish would benefit from flow visualization and computational simulations that can highlight interactions of vortical structure. By looking at those interactions, for example, we may understand why the thrust generated by the posterior-focused actuation did not increase for longer wavelengths (Fig. 5(b)) [31].

3) Advanced robotic swimmers: Building on the conclusion of this study that the two distinct kinematic patterns enable efficient underwater propulsion, further advances in robotic swimming can be made. For example, the number of the actuators can be reduced by designing a custom fluidic circuit to couple the actuators to generate the most efficient actuation modes revealed here, while using less power consumption. Also, exploring more design variables on top of the fixed actuation mode, such as the shape of the body, skin roughness [42], will provide opportunities to improve swimming performance such as speed and thrust.

Acknowledgment

The authors would like to acknowledge the members of the Serpent MURI team for their helpful comments and discussions related to this work, including Prof. Rob Shepherd, Prof. Mark Campbell, Prof. John Hwang, Prof. Ximin He, Prof. Lynden Archer, Prof. Willy Bemis, and the members of their groups.

REFERENCES

[1] J. C. Liao, "A review of fish swimming mechanics and behaviour in altered flows," *Philosophical transactions of the royal society b: biological sciences*, vol. 362, no. 1487, pp. 1973–1993, 2007.

[2] R. E. Shadwick and S. Gemballa, "Structure, kinematics, and muscle dynamics in undulatory swimming," *Fish physiology*, vol. 23, pp. 241–280, 2005.

[3] B. Dean and B. Bhushan, "Shark-skin surfaces for fluid-drag reduction in turbulent flow: a review," *Philosophical Transactions of the Royal Society A: Mathematical, Physical and Engineering Sciences*, vol. 368, no. 1929, pp. 4775–4806, 2010.

[4] A. J. Ijspeert, "Biorobotics: Using robots to emulate and investigate agile locomotion," *science*, vol. 346, no. 6206, pp. 196–203, 2014.

[5] D. Lattanzi and G. Miller, "Review of robotic infrastructure inspection systems," *Journal of Infrastructure Systems*, vol. 23, no. 3, p. 04017004, 2017.

[6] A. Vasilijević, . Na, F. Mandić, N. Mišković, and Z. Vukić, "Coordinated navigation of surface and underwater marine robotic vehicles for ocean sampling and environmental monitoring," *IEEE/ASME transactions on mechatronics*, vol. 22, no. 3, pp. 1174–1184, 2017.

[7] Y. Wang, G. Su, J. Li, Q. Guo, Y. Miao, and X. Zhang, "Robust, healable, self-locomotive integrated robots enabled by noncovalent assembled gradient nanostructure," *Nano Letters*, vol. 22, no. 13, pp. 5409–5419, 2022.

[8] G. Polverino, V. R. Soman, M. Karakaya, C. Gasparini, J. P. Evans, and M. Porfiri, "Ecology of fear in highly invasive fish revealed by robots," *Iscience*, vol. 25, no. 1, 2022.

[9] G. V. Lauder and E. D. Tytell, "Hydrodynamics of undulatory propulsion," *Fish physiology*, vol. 23, pp. 425–468, 2005.

[10] A. Jusufi, D. M. Vogt, R. J. Wood, and G. V. Lauder, "Undulatory swimming performance and body stiffness modulation in a soft robotic fish-inspired physical model," *Soft robotics*, vol. 4, no. 3, pp. 202–210, 2017.

[11] R. K. Katzschmann, J. DelPreto, R. MacCurdy, and D. Rus, "Exploration of underwater life with an acoustically controlled soft robotic fish," *Science Robotics*, vol. 3, no. 16, p. eaar3449, 2018.

[12] J. Zhu, C. White, D. K. Wainwright, V. Di Santo, G. V. Lauder, and H. Bart-Smith, "Tuna robotics: A high-frequency experimental platform exploring the performance space of swimming fishes," *Science Robotics*, vol. 4, no. 34, p. eaax4615, 2019.

[13] D. Q. Nguyen and V. A. Ho, "Anguilliform swimming performance of an eel-inspired soft robot," *Soft Robotics*, vol. 9, no. 3, pp. 425–439, 2022.

[14] J. D. Altringham and D. J. Ellerby, "Fish swimming: patterns in muscle function," *Journal of Experimental Biology*, vol. 202, no. 23, pp. 3397–3403, 1999.

[15] V. Di Santo, E. Goerig, D. K. Wainwright, O. Akanyeti, J. C. Liao, T. Castro-Santos, and G. V. Lauder, "Convergence of undulatory swimming kinematics across a diversity of fishes," *Proceedings of the National Academy of Sciences*, vol. 118, no. 49, p. e2113206118, 2021.

[16] G. V. Lauder, "Fish locomotion: recent advances and new directions," *Annual review of marine science*, vol. 7, no. 1, pp. 521–545, 2015.

[17] S. Currie and D. H. Evans, *The physiology of fishes*. CRC Press, 2020.

[18] P. Amal, A. R. Nair, H. Arunav, R. Raj, V. Akhil, C. Tawk, and K. V. Shankar, "Bioinspiration and biomimetics in marine robotics: a review on current applications and future trends," *Bioinspiration & Biomimetics*, 2024.

[19] H. Feng, Y. Sun, P. A. Todd, and H. P. Lee, "Body wave generation for anguilliform locomotion using a fiber-reinforced soft fluidic elastomer actuator array toward the development of the eel-inspired underwater soft robot," *Soft Robotics*, vol. 7, no. 2, pp. 233–250, 2020.

[20] A. Anastasiadis, L. Paez, K. Melo, E. D. Tytell, A. J. Ijspeert, and K. Mulleners, "Identification of the trade-off between speed and efficiency in undulatory swimming using a bio-inspired robot," *Scientific Reports*, vol. 13, no. 1, p. 15032, 2023.

[21] J. Cervera-Torralba, Y. Kang, E. M. Khan, I. Adibnazari, and M. T. Tolley, "Lost-core injection molding of fluidic elastomer actuators for the fabrication of a modular eel-inspired soft robot," in *2024 IEEE 7th International Conference on Soft Robotics (RoboSoft)*. IEEE, 2024, pp. 971–976.

[22] F. S. S. Inc., "Bend sensor technology mechanical application design guide," 2016.

[23] V. Stin, R. Godoy-Diana, X. Bonnet, and A. Herrel, "Form and function of anguilliform swimming," *Biological Reviews*, 2024.

[24] U. K. Müller, E. J. Stamhuis, and J. J. Videler, "Riding the waves: the role of the body wave in undulatory fish swimming," *Integrative and Comparative Biology*, vol. 42, no. 5, pp. 981–987, 2002.

[25] Q. Zhu, M. Wolfgang, D. Yue, and M. Triantafyllou, "Three-dimensional flow structures and vorticity control in fish-like swimming," *Journal of Fluid Mechanics*, vol. 468, pp. 1–28, 2002.

[26] O. Akanyeti, V. Di Santo, E. Goerig, D. K. Wainwright, J. C. Liao, T. Castro-Santos, and G. V. Lauder, "Fish-inspired segment models for undulatory steady swimming," *Bioinspiration & Biomimetics*, vol. 17, no. 4, p. 046007, 2022.

[27] L. Wen, T. Wang, G. Wu, and J. Liang, "Quantitative thrust efficiency of a self-propulsive robotic fish: Experimental method and hydrodynamic investigation," *IEEE/Asme Transactions on Mechatronics*, vol. 18, no. 3, pp. 1027–1038, 2012.

[28] Y.-J. Park, U. Jeong, J. Lee, S.-R. Kwon, H.-Y. Kim, and K.-J. Cho, "Kinematic condition for maximizing the thrust of a robotic fish using a compliant caudal fin," *IEEE Transactions on Robotics*, vol. 28, no. 6, pp. 1216–1227, 2012.

[29] P. L. Nguyen, B. R. Lee, and K. K. Ahn, "Thrust and swimming speed analysis of fish robot with non-uniform flexible tail," *Journal of Bionic Engineering*, vol. 13, no. 1, pp. 73–83, 2016.

[30] S. Ramananarivo, R. Godoy-Diana, and B. Thiria, "Passive elastic mechanism to mimic fish-muscle action in anguilliform swimming," *Journal of the royal society interface*, vol. 10, no. 88, p. 20130667, 2013.

[31] L.-M. Chao, M. M. Alam, and L. Cheng, "Hydrodynamic performance of slender swimmer: effect of travelling wavelength," *Journal of Fluid Mechanics*, vol. 947, p. A8, 2022.

[32] T. Namshad, M. Shrivastava, A. Agrawal, and A. Sharma, "Effect of wavelength of fish-like undulation of a hydrofoil in a free-stream flow," *Sādhanā*, vol. 42, pp. 585–595, 2017.

[33] A. Anastasiadis, A. Rossi, L. Paez, K. Melo, E. D. Tytell, A. J. Ijspeert, and K. Mulleners, "Eel-like robot swims more efficiently with increasing joint amplitudes compared to constant joint amplitudes," *Physical Review Fluids*, vol. 9, no. 11, p. 110509, 2024.

[34] A. J. Ijspeert and A. Crespi, "Online trajectory generation in an amphibious snake robot using a lamprey-like central pattern generator model," in *Proceedings 2007 IEEE International Conference on Robotics and Automation*. IEEE, 2007, pp. 262–268.

[35] S. E. Fetherstonhaugh, Q. Shen, and O. Akanyeti, "Automatic segmentation of fish midlines for optimizing robot design," *Bioinspiration & Biomimetics*, vol. 16, no. 4, p. 046005, 2021.

[36] C. D. Onal, X. Chen, G. M. Whitesides, and D. Rus, "Soft mobile robots with on-board chemical pressure generation," in *Robotics Research: The 15th International Symposium ISRR*. Springer, 2017, pp. 525–540.

[37] W. Coral, C. Rossi, O. M. Curet, and D. Castro, "Design and assessment of a flexible fish robot actuated by shape memory alloys," *Bioinspiration & biomimetics*, vol. 13, no. 5, p. 056009, 2018.

[38] C. Eloy, "On the best design for undulatory swimming," *Journal of Fluid Mechanics*, vol. 717, pp. 48–89, 2013.

[39] R. Wang, C. Zhang, Y. Zhang, L. Yang, W. Tan, H. Qin, F. Wang, and L. Liu, "Fast-swimming soft robotic fish actuated by bionic muscle," *Soft Robotics*, vol. 11, no. 5, pp. 845–856, 2024.

[40] P. Domenici and R. W. Blake, "The kinematics and performance of fish fast-start swimming," *Journal of Experimental Biology*, vol. 200, no. 8, pp. 1165–1178, 1997.

[41] S. Coombs, J. Bak-Coleman, and J. Montgomery, "Rheotaxis revisited: a multi-behavioral and multisensory perspective on how fish orient to flow," *Journal of Experimental Biology*, vol. 223, no. 23, p. jeb223008, 2020.

[42] G. Li, U. K. Müller, J. L. van Leeuwen, and H. Liu, "Body dynamics and hydrodynamics of swimming fish larvae: a computational study," *Journal of Experimental Biology*, vol. 215, no. 22, pp. 4015–4033, 2012.